AD-A116 989 HUGHES RESEARCH LABS MALIBU CA F/G 20/6
A COHERENT FIBER FOR AN AIRBORNE HETERODYNE SENSOR.(U)
APR 82 J A HARRINGTON DAAK80-81-C-0155
UNCLASSIFIED DAVAA-TR-81-0155-01 NL

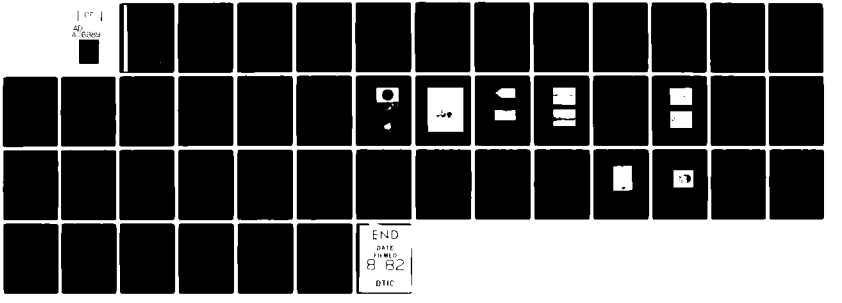

(12)

A COHERENT FIBER FOR AN AIRBORNE HETERODYNE SENSOR

J. A. Harrington

Hughes Research Laboratories
3011 Malibu Canyon Road
Malibu, CA 90265

April 1982

DAAK80-81-C-0155
Semiannual Report
For Period August 1981 through February 1982

Sponsored By
U.S. ARMY AVIONICS RESEARCH AND DEVELOPMENT COMMAND
Building 2525
Fort Monmouth, NJ 07703

UNCLASSIFIED

SECURITY CLASSIFICATION OF THIS PAGE (When Data Entered)

REPORT DOCUMENTATION PAGE	READ INSTRUCTIONS BEFORE COMPLETING FORM
1. REPORT NUMBER: TR 81-0155-01	2. GOVT ACCESSION NO. A116989 — 3. RECIPIENT'S CATALOG NUMBER
4. TITLE (and Subtitle): A COHERENT FIBER FOR AN AIRBORNE HETERODYNE SENSOR	5. TYPE OF REPORT & PERIOD COVERED: Aug. 1981 - Feb. 1982
	6. PERFORMING ORG. REPORT NUMBER
7. AUTHOR(s): James A. Harrington	8. CONTRACT OR GRANT NUMBER(s): DAAK80-81-C-0155
9. PERFORMING ORGANIZATION NAME AND ADDRESS: Hughes Research Laboratories, 3011 Malibu Canyon Road, Malibu, CA 90265	10. PROGRAM ELEMENT, PROJECT, TASK AREA & WORK UNIT NUMBERS: C12202AH45.01.11.01
11. CONTROLLING OFFICE NAME AND ADDRESS: U.S. Army Avionics Research & Development Command, Building 2525, Fort Monmouth, NJ 07703, Attn: DAVAA-E A. Kleider	12. REPORT DATE: April 1982
	13. NUMBER OF PAGES: 49
14. MONITORING AGENCY NAME & ADDRESS(if different from Controlling Office)	15. SECURITY CLASS (of this report): UNCLASSIFIED
	15a. DECLASSIFICATION DOWNGRADING SCHEDULE

16. DISTRIBUTION STATEMENT (of this Report)

Approved for public release: Distribution Unlimited.

17. DISTRIBUTION STATEMENT (of the abstract entered in Block 20, if different from Report)

18. SUPPLEMENTARY NOTES

19. KEY WORDS (Continue on reverse side if necessary and identify by block number)

Infrared Fibers
Fiber Optics
Fiber Optic Materials
Fiber Optic Sensors
Single Mode Fibers

20. ABSTRACT (Continue on reverse side if necessary and identify by block number)

Three approaches have been chosen for the fabrication of a 10.6 μm coherent fiber. The first approach involves cladding our thallium halide fibers either during extrusion or in a separate post-extrusion process. The second approach relies on the successful development of a new 10.6-μm transparent glass, $ZnCl_2$. The most speculative approach,

DD FORM 1 JAN 73 1473 EDITION OF 1 NOV 65 IS OBSOLETE

UNCLASSIFIED

SECURITY CLASSIFICATION OF THIS PAGE (When Data Entered)

derived from planar technology, requires that a cladding stripe be deposited on a ribbon of KRS-5 or other thallium halide.

During the first six months of the program we worked on the first two approaches. We attempted to coextrude single-mode fiber from a composite clad-core billet. Unfortunately, the clad-core interface of the extruded fiber was very irregular after every coextrusion attempted. We thus are abandoning this approach. The $ZnCl_2$ glass remains unstable (devitrifies) on exposure to atmospheric moisture. We are continuing our studies to stabilize the glass by adding various dopants.

TABLE OF CONTENTS

SECTION		PAGE
	LIST OF ILLUSTRATIONS	5
1	INTRODUCTION AND SUMMARY	9
2	COEXTRUSION OF THALLIUM HALIDE FIBERS	11
	A. Introduction	11
	B. Single Mode Fiber Design Considerations	11
	C. Experimental Procedures	15
	D. Experimental Results	18
3	ZINC CHLORIDE GLASS	27
	A. Background and Theoretical Considerations	27
	B. Experimental Approach to the Preparation and Characterization of $ZnCl_2$	36
4	FUTURE PLANS AND RECOMMENDATIONS	47
	A. Extrusion of Thallium Halide Fibers	47
	B. Zinc Chloride Glass	47
	REFERENCES	49

LIST OF ILLUSTRATIONS

FIGURE		PAGE
1	Index profiles for IR fibers	14
2	Clad/core billet for coextrusion of single mode IR fiber	16
3	Spindling cladding billets for fabrication into clad-core billets	17
4	TlBr/KRS-5 fiber showing irregular core shape	20
5	Enlargement of fiber cross section showing highly irregular core	21
6	TlBr/KRS-5 billet after extrusion	22
7	Side view of TlBr/KRS-5 fiber extruded at high temperature (300°C)	23
8	KRS-6/TlCl extruded fiber revealing the irregularly shaped core	25
9	Concentration (m) of saturated aquesou solution of $ZnCl_2 \cdot nH_2O$	28
10	Vapor pressure P(mm) of aqueous solution of anhydrous $ZnCl_2$ t 29.6°C as a function of concentration m	29
11	Vapor pressure P(mm) of aqueous solution as a function of concentration m of anhydrous zinc chloride, $ZnCl_2$, at 100°C	32
12	The three stages in the water uptake of solids from the vapor phase	33
13	Diagram of the set-up for the RAP synthesis of $ZnCl_2$	38
14	Close-up of reaction chamber showing Zn pellets, the gas inlet and the distillation outlet for $ZnCl_2(g)$	39
15	Ampoules of $ZnCl_2$ (vitreous)	40

FIGURE PAGE

16 DTA thermogram of RAP $ZnCl_2$ (sealed capsule) showing glass transformation at 120°C, devitrification at 190°C, and fusion at 310°C 44

17 DTA thermograms of non-RAP $ZnCl_2$ in sealed capsule 45

PREFACE

This semiannual report describes our initial progress on the development of a coherent fiber for use in a 10.6-μm heterodyne sensor system. The six-month period covered is from 27 August 1981 to 27 February 1982.

In addition to the principal investigator, James A. Harrington, others participating in the research program were: R.C. Pastor, L.E. Gorre, and M. Robinson in the $ZnCl_2$ glass studies; and R. Turk in the taking of photomicrographs. Overall managerial assistance and supervision was provided by L.G. DeShazer.

This research is being supported by the U.S. Army Avionics Research and Development Command, Fort Monmouth, NJ. The program is under the technical supervision of Dr. Al Kleider, AVRADA.

SECTION 1

INTRODUCTION AND SUMMARY

Our past development of infrared (IR) transmissive waveguides has generally involved the extrusion of unclad KRS-5 (TlBrI) fiber. This fiber is necessarily multimode and thus unsuitable for the present application. To fabricate a clad, single-mode fiber, we have chosen three approaches. In the first approach, thallium halide fibers are clad either during extrusion or in a separate post-extrusion process. The second approach relies on the successful development of a new 10.6-μm transparent glass — $ZnCl_2$. Finally, the most speculative approach, derived from planar technology, requires that a cladding stripe be deposited on a ribbon of KRS-5 or other thallium halide. During the first six months of the program we worked on the first two approaches, with work on the third approach not planned until end of first year.

The coextrusion of a clad-core fiber is clearly the most direct approach to fabricating a single-mode fiber. Drawing on over six years of experience in the extrusion of polycrystalline KRS-5 fibers, we felt it was logical to begin our studies by attempting to extend our extrusion technology to the fabrication of clad fiber. In this method a clad billet is first made by physically inserting a core into a hollow cylinder of the cladding material. The composite billet is then extruded into fiber. Our composite billets were made of TlBr/KRS-5 and KRS-6/TlCl (clad/core). The extruded fiber had an o.d. of 250 μm and a core diameter of 25 to 50 μm. Unfortunately, due to the large amount of friction between the billet and extrusion die, the clad-core interface was always found to be irregular, even when the extrusion parameters (temperature, pressure, and speed) were widely varied. At this point in the program, we have decided to abandon the technique of coextrusion. Our future experiments in this area will involve cladding the already-extruded fiber. One method is post-extrusion cladding by ion-exchange; another is sheathing of the small diameter fiber core with a suitable clad.

Zinc chloride glass is an appealing alternative to extruded fiber because we are dealing with a glass rather than the intrinsically more difficult thallium halide crystals. A glass may be readily drawn into fiber and is more easily clad than our crystalline materials. The problem is the highly

deliquiescent nature of $ZnCl_2$. This material has not yet been made in a form which is stable against even short (<10 min) exposures to atmospheric moisture. Therefore, our approach has been first to study the chemistry of this unique compound and, in particular, to attempt to develop means to stabilize the glass. The most general method is the application of our reactive atmosphere process (RAP) techniques to prepare a highly purified $ZnCl_2$ material. RAP techniques have been used very successfully to significantly reduce OH^- and other anion and cation impurities in metal halides and, therefore, it is reasonable to suspect that similar methods applied to $ZnCl_2$ would produce a highly purified state of $ZnCl_2$ which would be significantly less susceptible to moisture. (This was the case observed for RAP-prepared KCl crystals.) We found, however, that the pure RAP $ZnCl_2$ glass was not much more stable than non-RAP $ZnCl_2$ when exposed to the ambient atmosphere. While the time to devitrification and subsequent deliquescence was increased from several seconds in commerical- grade $ZnCl_2$ to several minutes for our RAP $ZnCl_2$, the glass is not yet stable enough to be useful for fabrication into fiber. Our future experiments will combine RAP chemistry and dopants, such as KCl, $PbCl_2$, ZnSe, and $GaCl_3$, to hopefully prepare a more stable product.

SECTION 2

COEXTRUSION OF THALLIUM HALIDE FIBERS

A. INTRODUCTION

There are several approaches to cladding thallium halide fibers. The simplest, conceptually, is the direct extrusion of a clad-core billet into single-mode fibers. In this method, the core material, such as KRS-5, is inserted into a hollow cylinder of cladding materials, such as TlBr. The composite billet, which is analogous to a preform in glass fiber drawing, is then coextruded into a clad fiber. Besides being a straightforward, one-step approach, this method of coextrusion takes advantage of our existing extrusion presses and of our technology developed over six years of extruding unclad polycrystalline fibers. Initially, therefore, we began our cladding investigation by developing coextrusion methods for the thallium halide fibers.

B. SINGLE MODE FIBER DESIGN CONSIDERATIONS

The fabrication of a single mode waveguide requires cladding and core materials with only slightly different indices of refraction. Typically, the difference in the refractive index, Δn, between the clad (n_2) and core (n_1) materials is 0.5 to 1.0%. In terms of the parameter Δ,

$$\Delta = \frac{n_1^2 - n_2^2}{2n_1^2} \approx \frac{n_1 - n_2}{n_1} \quad , \quad \text{for } \Delta \ll 1 \quad .$$

This normally means that $0.01 < \Delta < 0.02$. For the crystalline materials we use to make 10.6-μm transmitting fibers, the range of Δ's is considerably restricted because there are so few compatible materials. Furthermore, it is not readily apparent how one would easily grade the index of a crystalline

Table 1. Refractive indices of Thallium Halides

Material	Index of Refraction (10 μm)
KRS-6 (TlBrCl)	2.176
TlCl	2.193
TlBr	2.330
KRS-5 (TlBrI)	2.369

material, as is done in glass preform fabrication. Therefore, we have initially confined our choices to the materials listed in Table 1. Fortunately, we see from this table that there are several combinations of clad and core materials suitable for fabrication into a clad fiber. These combinations are summarized in Table 2. The results in Table 2 show that there are really only two viable clad/core combinations for fabrication of single-mode fibers. (Not all possible combinations for the four materials given in Table 1 are listed in Table 2. KRS-5 is listed with other halide materials for illustration purposes, even though only a TlBr clad is suitable for a coherent fiber.) The two combinations are TlBr/KRS-5 and KRS-6/TlCl. For these combinations, Δ is small enough to produce a core diameter sufficiently large to accept the 10.6-μm laser radiation. Also given in Table 2 are the values of the numerical aperture, NA:

$$NA = \sqrt{n_1^2 - n_2^2} = n_1\sqrt{2\Delta} \quad . \qquad (2)$$

The index profile of our clad fibers is illustrated in Figure 1. In Figure 1(a), the unclad KRS-5 is shown for reference purposes. At our usual diameters, $2a = 250$ μm, this waveguide will support many modes. To calculate the number of modes, I_{total}, we first compute the V number for the fiber from

Table 2. Single Mode IR Fiber Geometries for a Step-Index Waveguide Operating at 10.6 μm

Core n_1	Clad n_2	Δn	Δ	Core Diameter 2a, μm	NA
KRS-5	TlBr	0.033	0.014	20.6	0.395
	TlCl	0.176	0.072	9.1	0.896
	KRS-6	0.193	0.078	8.7	0.937
	Air	1.369	0.411	3.8	1.0
TlCl	KRS-6	0.017	0.008	29.7	0.273

$$V = \frac{2\pi a}{\lambda} (n_1^2 - n_2^2)^{1/2}$$

$$= \frac{2\pi a}{\lambda} n_1 \sqrt{2\Delta} ,$$

$$= \frac{2\pi a}{\lambda} NA \qquad (3)$$

and then relate V to the total number of modes:

$$I_{total} = \frac{V^2}{2} . \qquad (4)$$

For the multimode fiber shown in Figure 1(a), with n_1 = 2.37 (KRS-5), n_2 = 1.0 (air), 2a = 250 μm, V = 160, and I_{total} = 12,600.

For a single-mode fiber, illustrated in Figure 1(b), V must be equal to or less than 2.405. This means, using Equation (3), that the diameter of the core, 2(a), will be too small for our application unless Δ is very much less than 1. We have calculated 2(a) and listed the results in Table 2. As noted above there are only two combinations, giving a core diameter large enough to be usable at 10.6 μm. The last index profile shown in Figure 1(c) will also provide a single-mode fiber. In this structure, the core index of refraction varies parabolically:

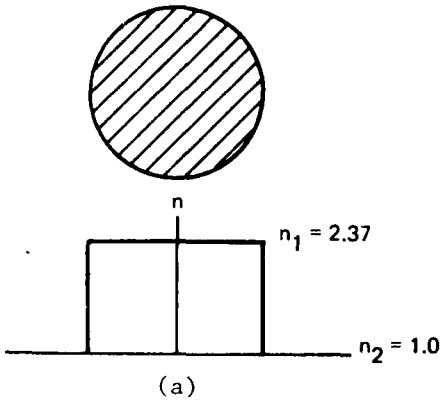

(a)

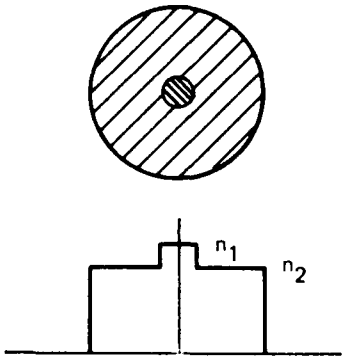

(b)

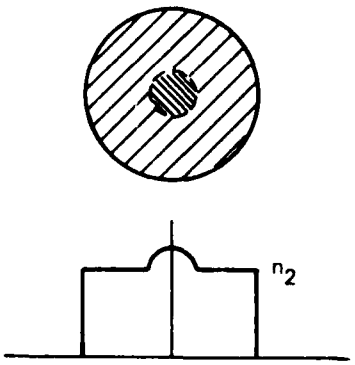

(c)

Figure 1.
Index profiles for IR fibers coextrusion of single mode IR fibers;
(a) "unclad" multimode KRS-5 fiber,
(b) step index waveguide, (c) graded index, parabolic profile.

$$n = n_1 \left[1 - \Delta \left(\frac{r}{a}\right)^2\right] \quad . \qquad (5)$$

For this case the core diameter would be twice as large as for the step-index profile shown in Figure 1(b). This would mean a core diameter of 59.4 μm for KRS-6/TlCl. The major problem we see with this profile is the difficulty in grading the index of our halide crystals. However, if this could be done, then the larger core diameter would greatly facilitate coupling of CO_2 laser radiation into the fibers.

C. EXPERIMENTAL PROCEDURES

The fabrication of a single mode fiber requires that the starting billet geometry be such that the extruded fibers have core diameters as indicated in Table 2. In Figure 2 we sketch the cross section of the appropriate billet geometry. The o.d. of the billet is 5.5 mm. With a billet core diameter of 0.5 mm, reduction to a 250-μm diameter fiber (extrusion ratio of 484:1) yields a fiber core diameter of 23 μm. This fiber core size is close to that indicated in Table 2 for the thallium halides.

The billet core size of 0.5 mm was chosen for convenience because this is the diameter of our standard extruded fiber. In principle, we can extrude any diameter of fiber required to form the exact single mode core size. At this point it seemed best to use our available fiber in the study of coextrusion methods.

The formation of the hole in the billet is important because the clad-core interface is a function of the surface quality of the hole and the fit of the core materials. To make a smooth, straight hole in the billet, we developed the spindling technique shown in Figure 3. We begin with either a single-crystal or polycrystalline solid billet. In the case of TlBr, which is quite soft, the use of a pre-compacted (polycrystalline) billet greatly facilitated the formation of a straight hole. This is because the polycrystalline material is harder than the single-crystal material. The first holes were made by spindling the

11772-1

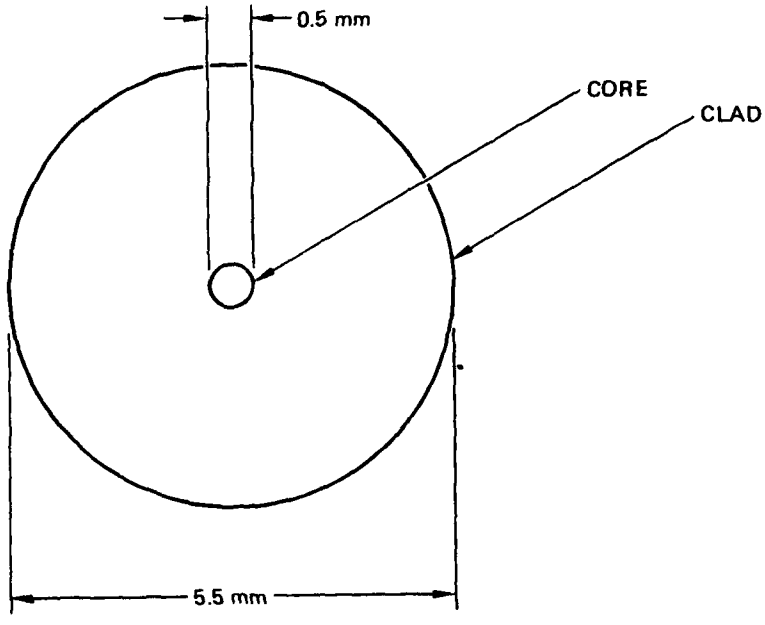

CORE : { KRS-5 } OR { TICl }
CLAD : { TlBr } { KRS-6 }

Figure 2. Clad/core billet for coextrusion of single mode IR fiber.

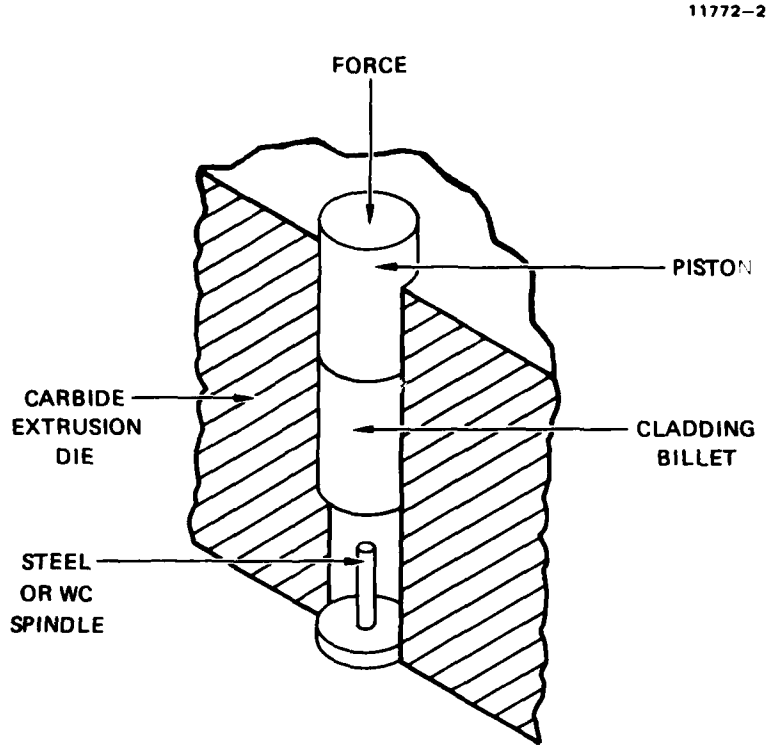

Figure 3. Spindling cladding billets for fabrication into clad-core billets.

billet in our extrusion press. This technique led to non-straight holes because the pins (made from hardened tool steel and tungsten carbide) bent after going only a short distance in the billet. This hole wander occurred even though the spindling was carried out at high temperatures (225 to 250°C) and slow compaction rates. The pins (0.5-mm diameter) were not strong enough to remain true and give a straight hole. To circumvent these problems, we went to a larger pin diameter (1.0 mm). In addition, we pre-drilled the billets with a slightly smaller hole, then spindled the billet onto the polished pin. The result was a straight, smooth hole.

The billets were loaded with 0.5- or 1.0-mm-diameter extruded fiber to form the final clad-core composite billet. This clad-core combination was then placed in our extrusion press for extrusion into 250-μm-diameter fiber. The extrusion temperature varied between 200 and 300°C, and the extrusion force from 5 to 20 kN (30,000 to 120,000 psi). After approximately one-half the billet was extruded, the process was stopped so that enough billet would be left for examination.

D. EXPERIMENTAL RESULTS

The majority of our studies were done on the TlBr-clad/KRS-5 core system. Because TlBr is softer (see Table 3 for hardness values of thallium halides) and more ductile than KRS-5, it would seem to be a good starting candidate for a cladding material. By selecting hard core and soft clad materials we would expect that the interface integrity would be more likely preserved because the soft clad would be less likely to deform the core in the fiber draw-down process.

Table 3. Hardness Values of the Thallium Halides

Material	Hardness (Knoop)
TlBr	11.9
TlCl	12.8
KRS-6	29.9
KRS-5	40.2

In Figure 4, we show photographs of the extruded fiber's cross section. The fiber pictured has been potted in plastic for polishing, then etched to reveal the grain boundaries. The most notable feature of these photographs is the irregularly shaped core (each photograph is from a different fiber end). At some points, the core appears to be shaped by the grain boundary. In other cases where the grain size is smaller, the core is still irregular, so we do not feel that the grains are tailoring the shape of the core. We also note from Figure 4 that the core diameter is approximately 25 μm, which is near the size predicted from our design considerations given in Section 2.B and 2.C. A large photograph (700X) of a typical fiber end face is shown in Figure 5.

The distortion of the fiber core results from large forces present during extrusion. Transverse forces present in the reduction cause the core to wander, and when combined with the compressive forces, lead to a highly irregular core. In Figure 6, the billet is photographed after extrusion. We observe here that the core is already somewhat deformed so that we cannot expect good fiber from this billet. That is, the squashed core in the billet resulting from frictional and compressive forces leads to fiber with a squashed core that tends to wander.

To better preserve the shape of the core, we tried two experiments designed to reduce the frictional and compressive forces. The first was a high temperature (300°C) extrusion. At 300°C, both materials are considerably softer than at 200°C. Thus, instead of using 15 to 20 KN force, we were able to extrude at 300°C using a force of only 3 kN. Unfortunately, the resultant fiber again had an irregular core (see Figure 7). In fact, the core in this case seems worse than fiber extruded near 200°C. This is likely due to the softness of the materials at these elevated temperatures. Thus, the advantage gained in reducing extrusion forces was lost due to the increased softness of the material. In the second experiment, we used a lubricant on the surface of the billet to reduce friction between the die body and billet. We selected Parafilm M as the lubricant because this turned out to be the best lubricant for the extrusion of KCl fiber. We wrapped a single layer of Parafilm M on the billet prior to extrusion at 130°C. The frictional

11772-3

(a) 200X

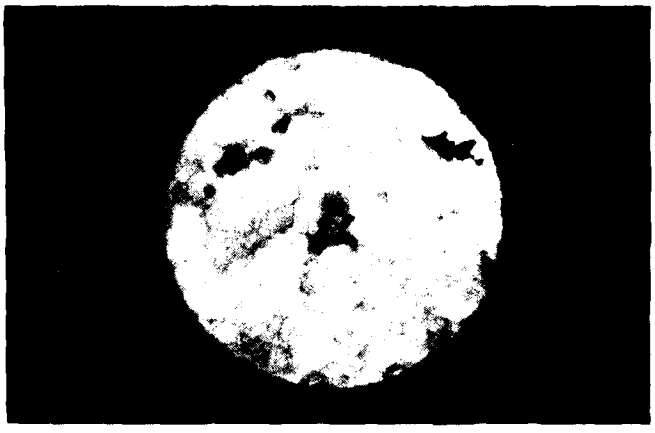

(b) 500X

(c) 1000X

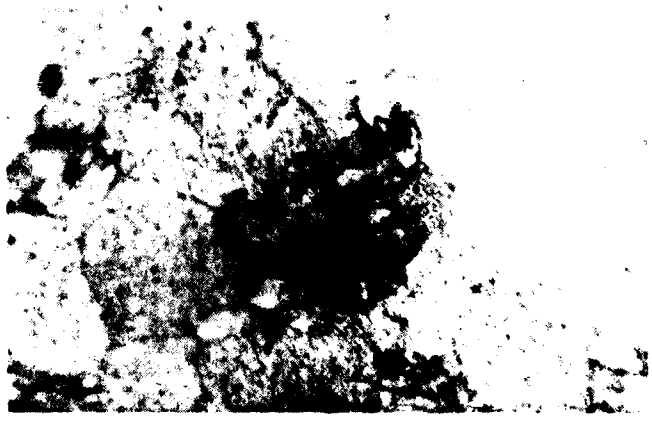

Figure 4. TlBr/KRS-5 fiber showing irregular core shape. Core diameter approximately 25 μm but interface is badly deformed.

11772-4

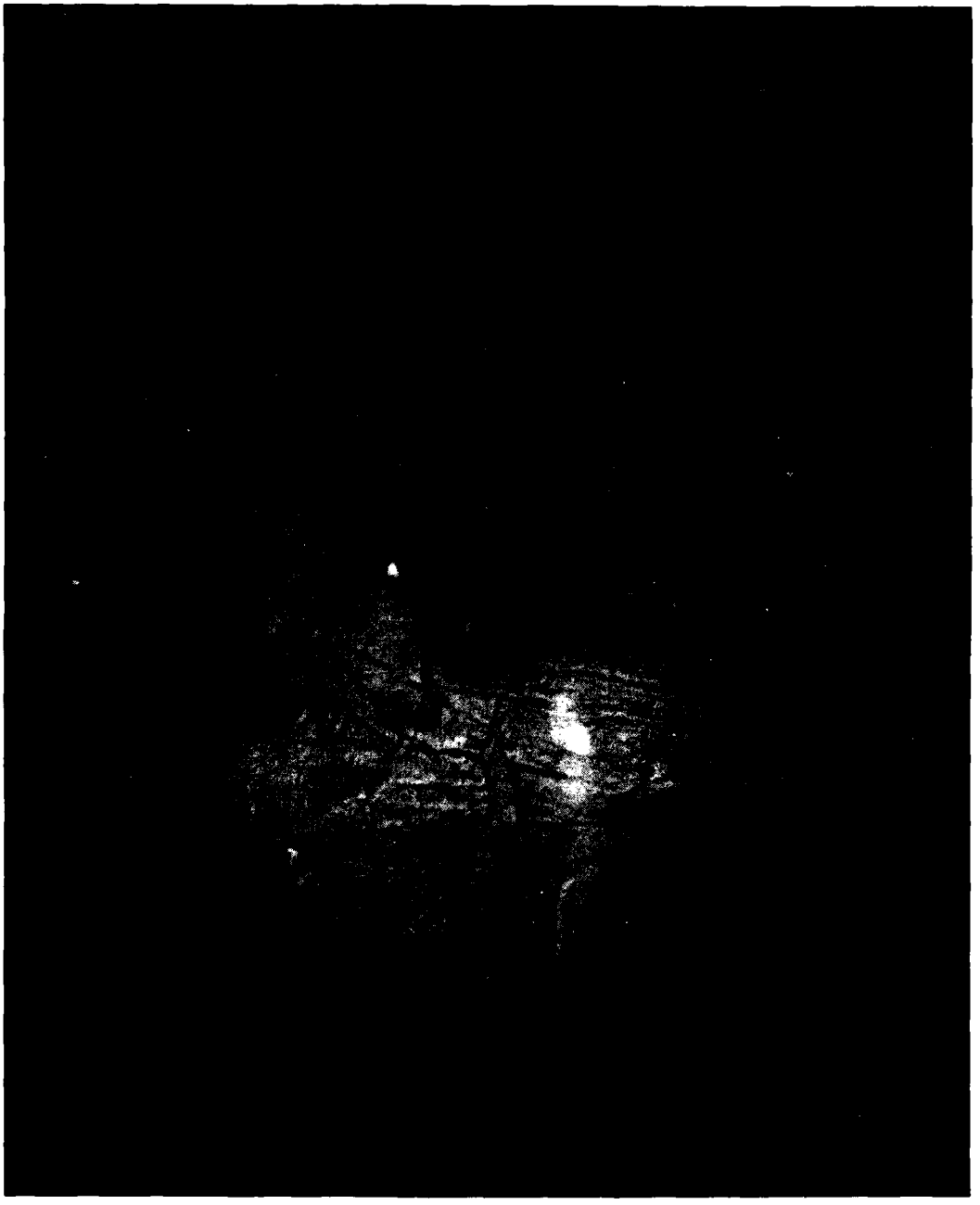

Figure 5. Enlargement of fiber cross section showing highly irregular core.

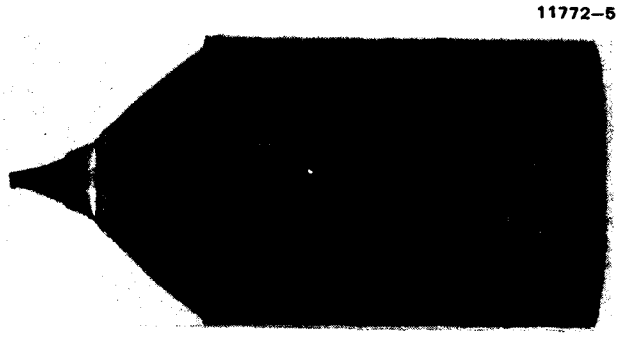

(a) 7.5X

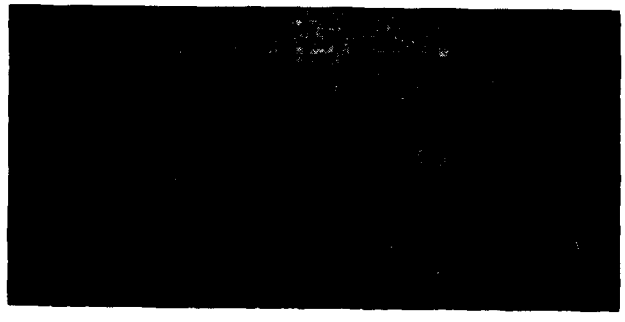

(b) 7.5X

Figure 6. TlBr/KRS-5 billet after extrusion. Core has been compressed and we can see the extrusion defect at the end of the billet. (a) is the entire billet; (b) is the same billet in cross-section.

11772-6

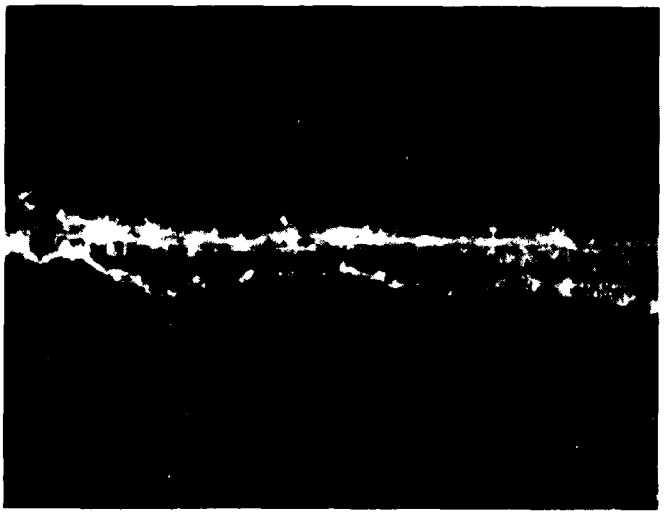

50X

100X

Figure 7. Side view of TlBr/KRS-5 fiber extruded at high temperature (300°C).

force was reduced significantly because less than 1 kN force was required to extrude the fiber. Again, the core was irregular although some improvement was noted.

As a final attempt at improving the clad-core interface, we decided to reverse the hardness of the materials used for the clad and core. From Table 3 we see that this is accomplished if we use a KRS-6 cladding and a TlCl core. The basic premise here is that the harder cladding will not be crushed as easily as the TlBr cladding and thus the KRS-6 will protect the soft TlCl core. The KRS-6/TlCl fiber extruded is shown in Figure 8. Because both of these materials are whitish in color, the core is not as visible as for TlBr/KRS-5. We do, however, again see the irregular core structure. The diameter is seen to vary and the core wanders.

The results of our coextrusion work clearly indicate the difficulty in producing a single-mode or even a clad fiber. At this point, we feel that further work using this coextrusion method is unwarranted. Therefore, we shall not pursue this approach any further.

50X

100X

Figure 8. KRS-6/TlCl extruded fiber revealing the irregularly shaped core.

SECTION 3

ZINC CHLORIDE GLASS

A. BACKGROUND AND THEORETICAL CONSIDERATIONS

Zinc chloride forms a glass which is transparent at 10.6 μm. Workers at Bell Telephone Laboratories made theoretical estimates of the losses in this glass and they predict an absorption coefficient near 10^{-4} cm^{-1} at 10 μm. They even were able to make some $ZnCl_2$ fiber. Unfortunately, $ZnCl_2$ is extremely sensitive to moisture and will rapidly devitrify then deliquesce in a matter of minutes. Our development of this material centers on stabilizing the glass against devitrification and subsequent deliquescence. Initially, this has involved using our RAP chemistry to purify the material. Most recently we have added dopants to further stabilize the glass.

The literature highlights deliquescence as the foremost problem in handling $ZnCl_2$. However, it is also stated that the anhydrous form is stable in contact with its saturated aqueous solution at temperatures above 28°C. The basis for this claim is seen in Figure 9 where the solubility line of the anhydrous form, $ZnCl_2$(solid), intersects that of $ZnCl_2 \cdot H_2O$(s) at 28°C. The solid line defines the temperature region for the existence of the stable form in contact with the saturated solution of $ZnCl_2 \cdot nH_2O$(s), where n goes from 4 to 0. Thus, to prevent deliquescence of the anhydrous crystal, materials handling of $ZnCl_2$(s) must be carried out above 28°C. How much above 28°C depends on the ambient humidity.

Table 4 shows how the water vapor pressure, P, of the solution changes with temperature, T, and concentration, as measured by molality, m. Molality, m, is the number of moles of solute per kg of solvent, and is related to mole fraction x of $ZnCl_2$ by: $x = m/(m + 55.51)$. Two of these temperatures, 29.6 and 100°C, are in the regime where anhydrous $ZnCl_2$(s) is the stable phase. For each temperature the relevant P value for gauging deliquescence is the value of the molality at saturation, m*. The saturation pressure of water at each temperature is given by P_o. Figure 10 shows how fast P decreases with increasing m at 29.6°C. At the saturation value of m* = 32.2 mol/kg at 29.6°C, the extrapolated value of $P \leq 1$ mm Hg.

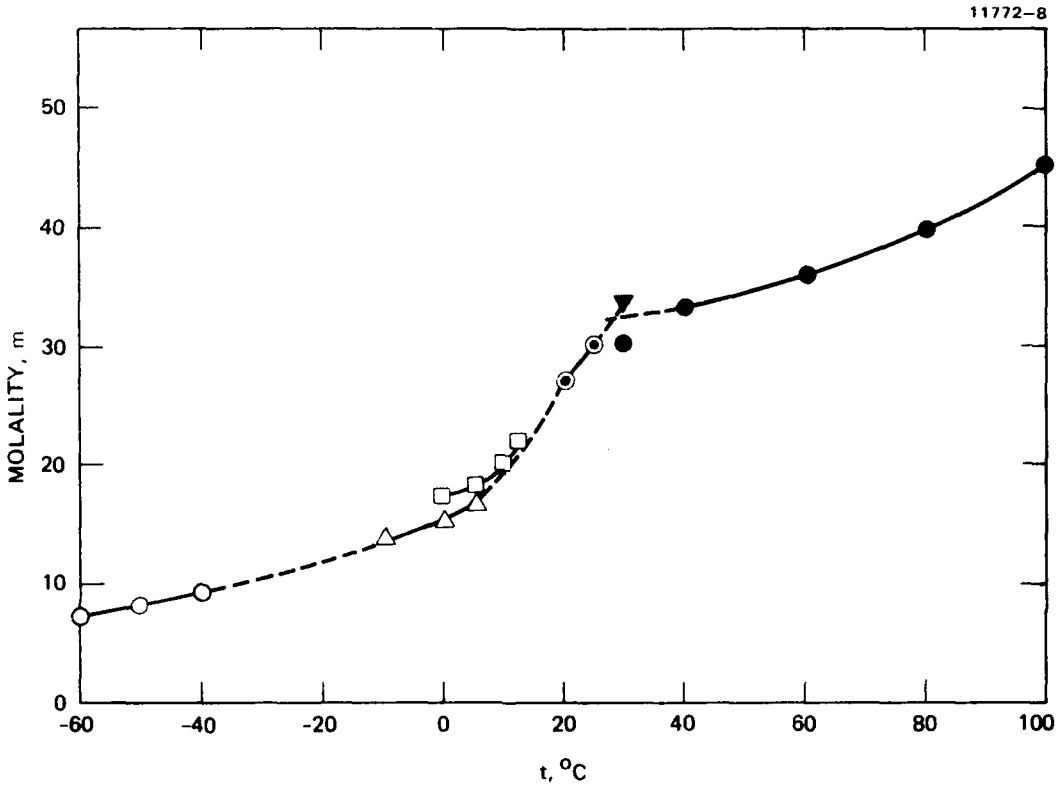

Figure 9. Concentration (m) of saturated aquesou solution of $ZnCl_2 \cdot nH_2O$ Legend for the solid phase ○, n = 4; △, n = 3; □, n = 5/2; ⊙, n = 3/2; ▼, n = 1; ●, n = 0. (Taken from I.C.T., Vol. IV, p. 221 (1928)).

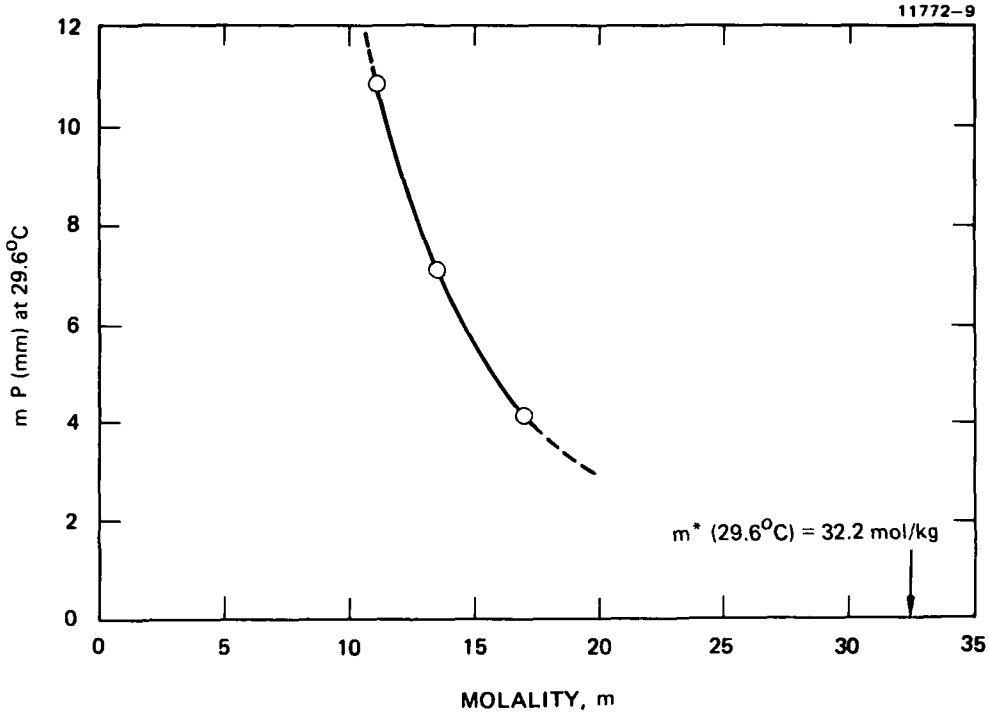

Figure 10. Vapor pressure P(mm) of aqueous solution of anhydrous $ZnCl_2$ at 29.6°C as a function of concentration m. For the saturated solution at 29.6° C, m* = 32.2 mol % (Taken from I.C.T., Vol. III, p. 294 (1928).)

At this point one might speculate that a higher temperature may be more compatible with an ambient, P, of 10 to 15 mm Hg. (Assuming an ambient temperature of 25°C where the vapor pressure of $H_2O(liq)$, P_o, is 23.75 mm, a relative humidity in the range 42 to 63% corresponds to P of 10 to 15 mm Hg.) Raising the temperature brings two competing factors. It is true that P* of the saturated solution increases with temperature, but so does m*, which lowers P*. Figure 11 gives the behavior of P versus m at 100°C. Note that at 100°C, m* = 45.1 m. The fast decline in P with an increase in m at 100°C compared to that at 29.6°C (cf. Figure 10) indicates a more unfavorable situation. What this means is that the thermal coefficient of m* predominates over the thermal coefficient of P.* This relation appears to hold for all deliquescent salts.

Solubility is a thermodynamic property; hygroscopic behavior and deliquescence are not. The distinction is appreciated in Figure 12. The lower leg of the S-shaped curve, (1), the induction period, refers to the time interval for conditions to occur at the interface to lower the energy barrier and usher in the kinetic uptake of H_2O, (2), which is deliquescence or just plain dissolution. The top part of the curve, (3), the plateau, is the thermodynamic limit of H_2O-uptake and is just a function of temperature and the external pressure. For our purpose, the solid $ZnCl_2(s)$ is useless the moment the induction period, (1), is over. Clearly, our problem is to lengthen the induction period, the time interval when the energy barrier to H_2O-uptake is abnormally high. The amount of lengthening sought, say about one hour, should enable one to bring to bear effective materials handling.

The hydroxide impurity OH^-, a pseudo-halide, is known to lower the energy barrier of the surface for H_2O-sorption to take place. The application of reactive atmosphere processing (RAP) to alkali and alkaline-earth metal halides provides a convenient method of removing OH^- from a material. The easy fogging which occurred in KCl windows when exposed to the environment was rectified by RAP. Fabricated pieces of RAP KCl have been exposed to the environment for several years with no sign of surface deterioration.

Table 4. The Vapor Pressure P of Aqueous Solutions of Zinc Chloride as a Function of Temperature T and Concentration m

T, °C/P_o, mm	Molality, mol/kg	P, mm
14.6, 12.46	11.0	4.37
	13.5	2.55
	17.0	1.41
	(23.2)*	(——)*
24.6/23.19	11.0	8.07
	13.5	5.10
	17.0	2.92
	(30.0)*	(——)*
29.6/31.09	11.0	10.8
	13.5	7.09
	17.0	4.20
	(32.2)*	(——)*
100/760	1.3	733
	2.7	695
	5.0	607
	7.0	513
	9.0	415
	(45.1)*	(——)*

*Values for the saturated solution.
International Critical Tables, Vol. III, p. 294 (1928).

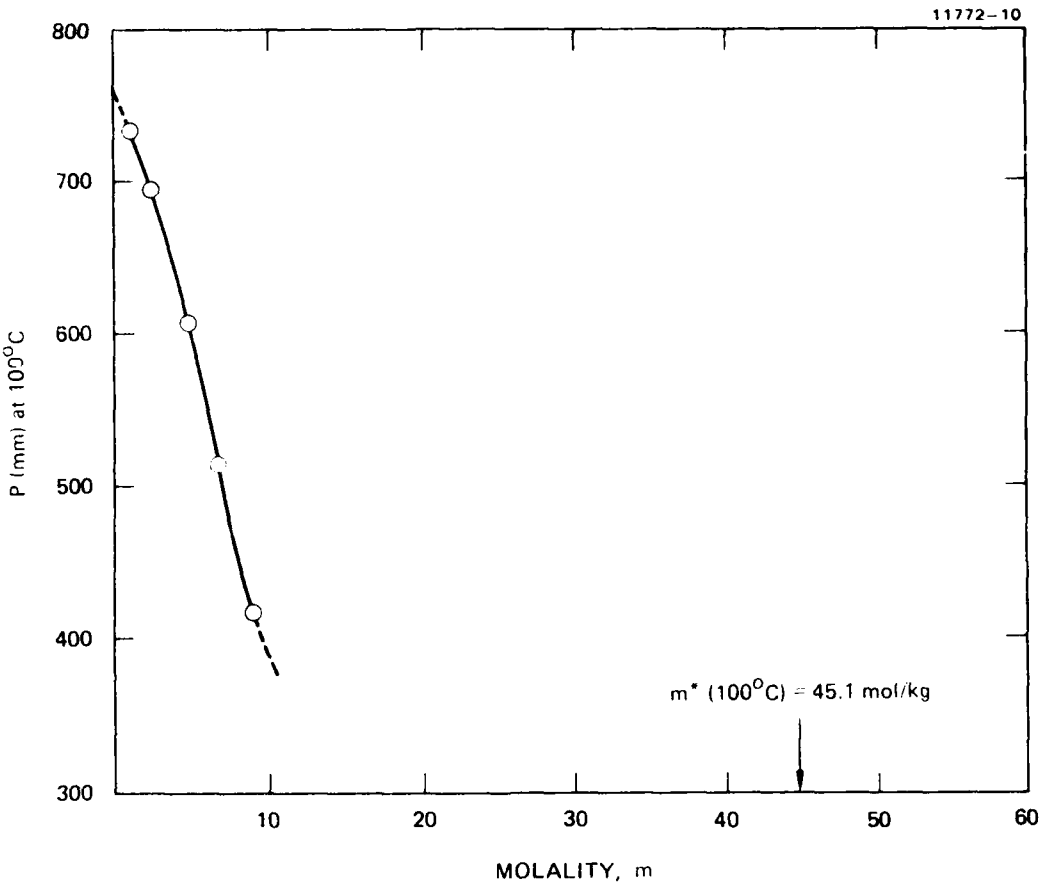

Figure 11. Vapor pressure P(mm) of aqueous solution as a function of concentration m of anhydrous zinc chloride, $ZnCl_2$, at 100°C. For the saturated solution at 100°C, m* = 45.1 mol % (Taken from I.C.T., Vol. III, p. 294 (1928).)

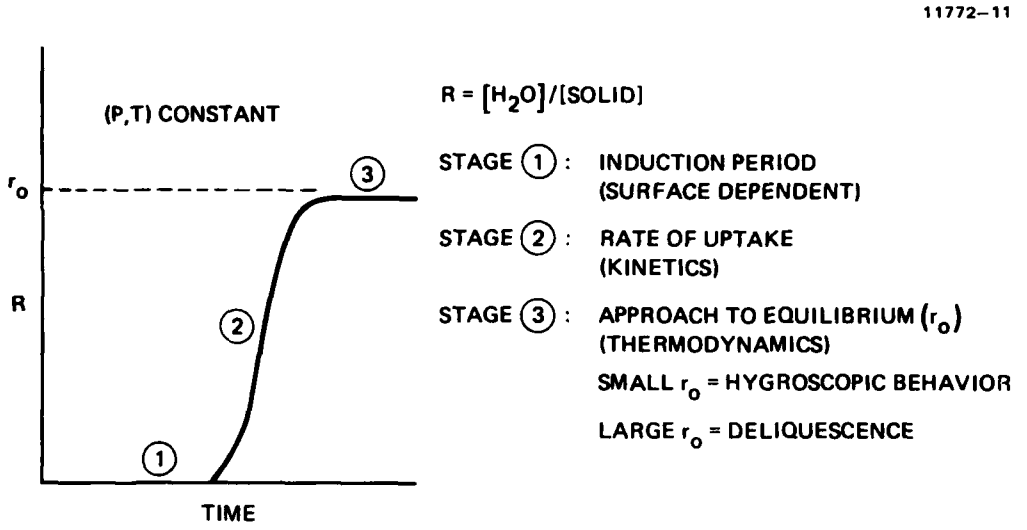

Figure 12. The three stages in the water uptake of solids from the vapor phase.

Consequently, a RAP procedure for the synthesis of $ZnCl_2$ was developed (cf. next section). Five-nines percent pure (99.999%) Zn pellets were reacted with CCl_4, thus

$$2Zn + CCl_4 \rightarrow 2ZnCl_2 + C \quad . \tag{6}$$

The product $ZnCl_2$ was distilled out. The vitreous state of $ZnCl_2$(vit) was readily obtained in the distillate. Upon exposure of RAP $ZnCl_2$(vit) to the environment, a distinct time lag to H_2O-uptake was noted, as compared to the conventional material. The effect may have been due to a reduced surface concentration of OH^- in the RAP material. On the other hand, the difference may have been due merely to a lower value of the specific surface (surface per unit weight) of the RAP $ZnCl_2$(vit).

Consequently, we considered another alternative, viz., the use of dopants, cations or anions. As discussed in the next section, glass formation of $ZnCl_2$ with 50 mole % KCl, as reported in the literature, did not occur under RAP. Easy crystallization from the liquid state resulted down to 10 mole % KCl. Under RAP, other dopants, such as $ThCl_4$ and $PbCl_2$ proved inapplicable. Anion doping with ZnS and ZnSe was extremely limited because of the low solubility in the $ZnCl_2$ melt. However, cation doping with $GaCl_3$ and anion doping with ZnSe prolonged the induction period to 6 to 9 min, a considerable extension.

It was at this phase of the study that the whole effort was transferred to the contract. We noted that invariably, upon exposure to the environment, devitrification,

$$ZnCl_2(vit) \rightarrow ZnCl_2(crystal) \quad , \tag{7}$$

an irreversible process, preceded the deliquescence. Thus, deliquescence was a problem of the crystalline state. The process in which the induction period should be extended is with respect to the surface-layer rearrangement shown by Equation (7). Of course, once devitrified, the material was useless and deliquescence was inconsequential.

To achieve a rapid exploration of the use of dopants, we designed a test-tube experiment (cf. next section) where CCl_4 and NH_4Cl vapors blanketed the

reactants, $ZnCl_2$, and the dopant. We observed that 2 mole % KCl was insufficient, i.e., the supercooled liquid devitrified. An extended induction period was seen in 5 mole % KCl. However, at 10 mole % KCl the liquid crystallized. A distinction is made between crystallization and devitrification, where the latter means that the vitreous state was observed before crystallization. Also, 2.5 mole % $PbCl_2$ looked promising. However, when these mixtures were adopted in the synthesis, under rigorous RAP, the melt crystallized. Thus, the test-tube experiments do not reproduce the RAP conditions required.

It appears from the results with KCl (or $PbCl_2$) that anion doping by OH^- may be assisting glass formation, presumably, through hydrogen-bonding, which yields a less-rigid network. Glass formation of $ZnCl_2$ with 50 mole % KCl has only been achieved by a rapid quench in air. We are not interested in OH^- or O^{-2} doping of $ZnCl_2$, since that would exact a tradeoff in the IR transparency. Besides, there is evidence which indicates that O^{-2} doping of RAP $ZnCl_2$ leads to easy devitrification (cf. next section).

The $ZnCl_2$ devitrification process we observed initiates at the surface. It is possible that the surface rearrangement is triggered by the heat of absorption of polar gas molecules, such as H_2O or HF. These two molecules are very similar because the pseudohalide, OH^-, is isoelectronic with F^- and is very close in ion size and electronegativity. Thus, the exposure of $ZnCl_2$(vit) to HF gas also effects devitrification readily, as in the case of H_2O. This behavior was observed in the attempt to passivate the surface of $ZnCl_2$(vit) by forming a thin layer (or film) of ZnF_2. Equation (7) shows that $ZnCl_2$(vit) has the higher free energy. Hence, the vitreous material will tolerate a lower value of $P(H_2O)$ than the crystalline form.

We can combat the tendency to devitrify by lowering the surface probability for occupancy by Zn^{+2} of adjacent sites. We have already seen that the approach based on bulk doping with KCl and $PbCl_2$ is not adequate. Unless there is a tendency for the dopant to concentrate on the surface, the site occupancy probability does not vary sensitively with bulk concentration. A 5-mole % doping lowers the site occupancy probability by only 10%.

However, we can lower the probability further by increasing the number of strong linkages per dopant. Note from the earlier part of the discussion that the only dopants which led to an extended induction period under rigorous RAP were gallium (in $GaCl_3$), which is capable of three strong linkages, and selenide (in ZnSe), which is capable of two strong linkages. If the model is correct, gallium selenide (Ga_2Se_3) would have been more effective.

B. EXPERIMENTAL APPROACH TO THE PREPARATION AND CHARACTERIZATION OF $ZnCl_2$

1. Introduction

Work on $ZnCl_2$ to date is limited by its tendency to deliquesce when exposed to the atmosphere. This kinetic behavior may not be intrinsic to the material but dependent on the presence of OH-impurities. If H_2O and its derived impurities are rigorously excluded during the synthesis of $ZnCl_2$, a superior material may result. Thus, high purity Zn metal and dry CCl_4 as the source of Cl were used to prepare $ZnCl_2$ in a H_2O-free environment.

The pyrolysis of CCl_4 follows two paths where Cl is favored over Cl_2 at a ratio of 4:1 from 600° to 900°C (Ref. 1).

$$CCl_4 \xrightarrow{20\%} C + Cl_2 \qquad (8)$$

$$CCl_4 \xrightarrow{80\%} \frac{1}{2} C_2Cl_6 + Cl \qquad (9)$$

To prevent incorporation of C, a byproduct of Equation (8), O_2 may be used as the carrier gas, since

$$C + \frac{1}{2} O_2 \rightarrow CO \quad . \qquad (10)$$

Contamination with ZnO is not a problem because the reaction below is thermodynamically unfavorable from 25°C to 1200°C, thus

$$ZnCl_2 + \frac{1}{2} O_2 \rightleftharpoons ZnO + Cl_2 \quad . \qquad (11)$$

Furthermore, a Cl_2:O_2 ratio greater than unity will favor the backward displacement of Equation (11).

2. Experimental Procedure

Figure 13 is a diagram of the set-up used in the synthesis. The vitreous silica apparatus is flamed at high temperatures under a N_2 flow to remove absorbed H_2O on the walls of the tube. Once cooled, a known weight of 99.999% Zn shots is loaded into the reaction chamber and the set-up heated under vacuum to further remove H_2O and also to pump-out occluded gases in Zn. When the Zn has melted and been degassed, pumping is stopped and the set-up is filled with the carrier gas, e.g., He, O_2 or He/O_2. Once there is a positive flow, the gas is made to sweep through Electronic Grade CCl_4(liq), previously dried with zeolite, into the Zn chamber which is heated to 610°C (where P_{ZnCl_2} = 100 mm). Figure 14 shows a closeup view of the reaction chamber. $ZnCl_2$(g) is subsequently distilled into the receiver, which is maintained at 400°C. At 400°C the $ZnCl_2$ is liquid and $P_{ZnCl_2} < 1$ mm Hg. Any unpyrolyzed CCl_4 is collected in a dry-ice-acetone trap and residual Cl_2 is neutralized in a NaOH scrubber. The reaction chamber and receiver are protected from the back diffusion of H_2O(g) from the NaOH scrubber by an intervening oil bubbler. When the reaction is complete, i.e., when the volume of distillate approximates the stoichiometric amount of $ZnCl_2$ obtainable from Zn, both reaction chamber and receiver are cooled down and the CCl_4 bypassed. The distillate in the ampoules, quenched in air, solidifies to form $ZnCl_2$(vit). The gas flow is stopped, the set-up evacuated to a few hundred microns and the ampoules tipped off. Figure 15 shows ampoules containing $ZnCl_2$ (vit) obtained by this process. The cause of the difference between the contents of the ampoules is explained in the next section.

3. Results and Discussion

The choice of carrier gas used in the synthesis evolved from a series of observations from several runs. Helium was originally used but black suspended particles would often be found in the distillate, as seen in

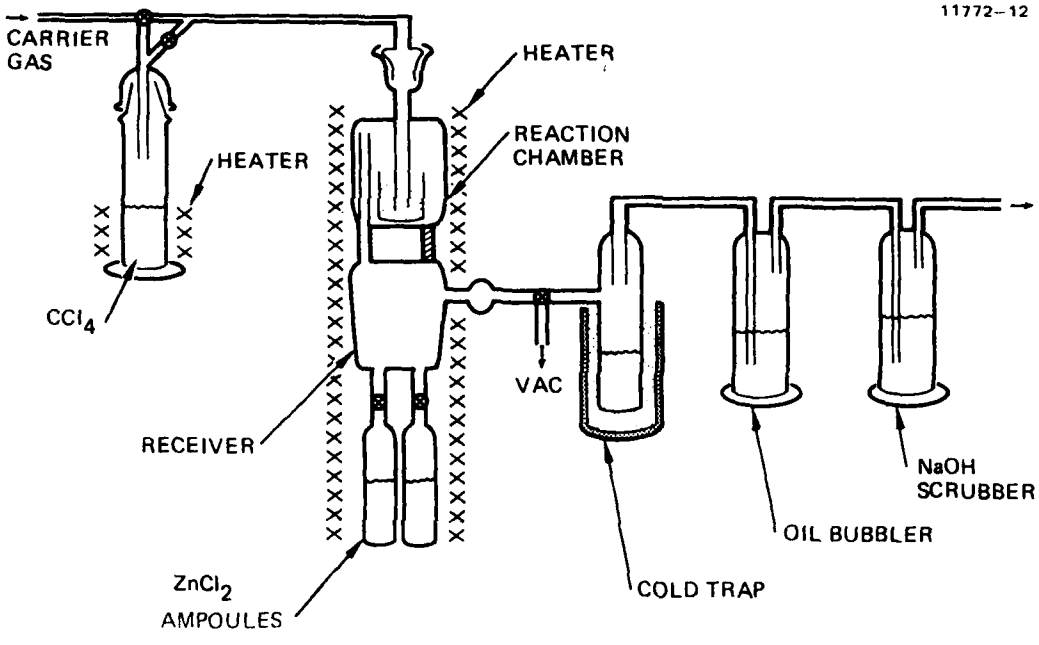

Figure 13. Diagram of the set-up for the RAP synthesis of $ZnCl_2$.

11772-13

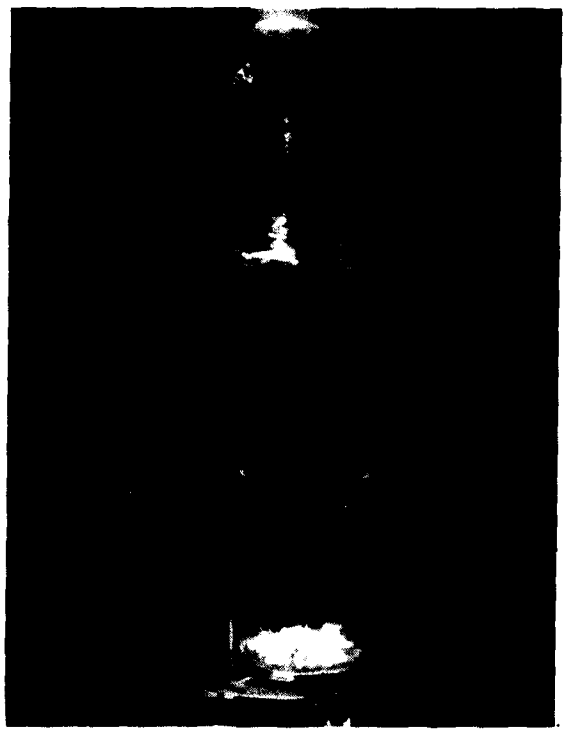

Figure 14.
Close-up of reaction chamber showing Zn pellets, the gas inlet and the distillation outlet for $ZnCl_2(g)$.

11772-14

a b c

Figure 15.
Ampoules of $ZnCl_2$ (vitreous): (a) water-white material. (b) with black suspended particles, and (c) purple material.

Figure 15(b). Assuming the black particles to be C, Equation (8), He was replaced by a mixture of He and O_2 for the latter to remove C (Equation (10)). However, it was noted that the black residue still appeared when the distillation rate was increased. At this point, O_2 was used as the carrier. The product obtained was yellowish and devitrified easily. The yellow color could have been due to a solvated hole formed from dissolved O_2 in the $ZnCl_2$ melt; thus,

$$\frac{1}{2}\ O_2(solv) + O^{-2}(solv) + 2\ \ (solv)\ \ . \qquad (12)$$

Upon reviewing the process parameters adopted in the runs using He and O_2/He, it was realized from the vapor density of Zn and the pyrolysis data on CCl_4 that the formation rate of $ZnCl_2$ was limited by the temperature of the CCl_4(liq) source, and not by the temperature of the reaction chamber. Zn(g) could have distilled over and been deposited in the ampoules and reacted with CCl_4 forming C, as shown in Equation (6). Thus, raising the temperature of the CCl_4 source yielded a faster reaction rate and produced water-white $ZnCl_2$(vit), as seen in Figure 15(a). Also, the melting of Zn under vacuum was, eliminated to prevent distillation of free Zn into the receiver, since this step of the synthesis was found to be superfluous, based on the negligible change in pressure at melting. Helium was therefore found to be the ideal carrier gas to use, O_2 being unnecessary and even deletrious to glass formation.

The speculation explaining the presence of C residue in the ampoules was further reinforced by the observation of a crust of C in the Zn container, suggesting a fast, heterogeneous reaction. This reaction, in fact, was faster than the distillation rate of $ZnCl_2$, as the chamber residue was $ZnCl_2$, and not unreacted Zn. Thus, the pyrolytic breakdown path of CCl_4, leading to the formation of atomic chlorine by Equation (9) was overwhelmed by Equation (6). The conjecture is supported by two observations: insignificant formation of Cl_2 and C_2Cl_6. Another observation which supports the reaction model of Equation (6) comes from the measured amount of unreacted CCl_4(liq): the CCl_4 consumed is at least three times more than what would have been lost by pyrolysis alone.

The distilled $ZnCl_2$ was originally sealed-off in silica ampoules under a CCl_4/He flow. However, at the seal-off region, a dark residue was formed which was partially soluble in $ZnCl_2(\ell)$, imparting a purple color to the solution, as seen in Figure 15(c), a behavior reminiscent of a solvated electron,

$$Zn(solv) \rightleftharpoons Zn^{+2}\ (solv) + 2e\ (solv)\ , \qquad (13)$$

where solv is $ZnCl_2(\ell)$. The thermodynamic models examined failed to come up with free Zn at the seal-off temperature. Kinetic considerations, employing bond energies as a measure of drive, indicate that the trichlormethyl radical, $\cdot CCl_3$, produced in the pyrolysis of CCl_4, Equation (9), reduces $ZnCl_2$ to Zn, thus

$$ZnCl_2 + 2\ CCl_3\cdot \rightarrow Zn + 2CCl_4\ . \qquad (14)$$

This leads to an energy increase of 1 kcal, which is easily accommodated at the seal-off temperature where RT = 4 kcal. The formation of the dark residue was avoided by removing $CCl_4(g)$ before seal-off.

The use of dopants was explored as a means to stabilize $ZnCl_2$(vit) against devitrification. The reported glass formation of $ZnCl_2$ with 50-mole % KCl was not realized in the RAP set-up. A reported similar behavior with KI was not examined because the RAP procedure would convert KI to KCl. To increase electron-pair donor density (Lewis base), ZnS and ZnSe were used; and for electron-pair acceptors (Lewis acid), CuCl, $GaCl_3$ were used. A starting composition of 2.4 mole % $GaCl_3$ blocked devitrification for nine minutes in room temperature air. Under the same environmental conditions, a control piece of undoped $ZnCl_2$(vit) devitrified immediately, i.e., <1 min.

Test tube experiments were carried out using $PbCl_2$ and KCl as dopants, with $ZnCl_2$ as the starting material, and NH_4Cl and CCl_4 providing HCl and Cl_2 in the atmosphere. $ZnCl_2$ with 2.5 mole % $PbCl_2$, and $ZnCl_2$ with 5 mole % KCl, formed a vitreous material with this method. Attempts to reproduce these compositions under RAP failed, resulting in crystalline products.

4. Thermal Characterization

Differential Thermal Analysis (DTA) characterization of the $ZnCl_2$ product (sealed capsule) in Figure 16 shows the classic behavior: the glass transformation temperature (T_g) occurs at ~120°C, devitrification (T_c) at 190°C, and fusion (T_f) at 310°C. Thus, the intrinsic tendency to devitrify at $P(H_2O) \simeq 0$ takes place at 190°C at a scan rate of 20°C/min. The devitrification temperature is expected to decrease with the scan rate or with an increase in $P(H_2O)$. This was found to be true, as evidenced by the DTA characterization of non-RAP $ZnCl_2$, Figure 17(c). The sample was prepared by melting $ZnCl_2$(crystal) following the test tube method previously described, then quenching in air. The vitreous $ZnCl_2$ was then transferred into a Pyrex capsule, pumped and sealed off. No attempt was made to rigorously exclude H_2O in the process. This particular sample showed T_c at 110°C and T_f at 180°C, 80°, and 130° lower than RAP $ZnCl_2$, respectively (see Figure 16).

In the same manner, DTA characterization was done on the test-tube-prepared 5% KCl in $ZnCl_2$ (Figure 17(a)), showing T_c at 85°C and T_f at 166°C: and for 2.5% $PbCl_2$ in $ZnCl_2$ (Figure 17(b), showing T_c at 80°C and T_f at 200°C. Unlike the undoped $ZnCl_2$ of Figure 17(c) which showed a clean melting endotherm, those of the doped $ZnCl_2$ exhibited extra structures which may be attributed to the dissolution of KCl or $PbCl_2$ in the $ZnCl_2$ melt. All three thermograms in Figure 17 did not show glass transformation above 40°C, which implies that these materials were soft at temperatures as low as 40°C.

The $ZnCl_2$ glasses characterized in Figure 17 being formed at a nonzero value of $P(H_2O)$ contain a significant amount of OH^-. Under RAP, where $P(H_2O) \simeq 0$, the KCl or $PbCl_2$ doping does not yield the vitreous state. Hence, we conclude that the glass formation of Figures 17(a) and 17(b) were assisted by hydrogen bonding. The latter, a weak bond, would lower the value of T_f, T_c, and T_g, as observed.

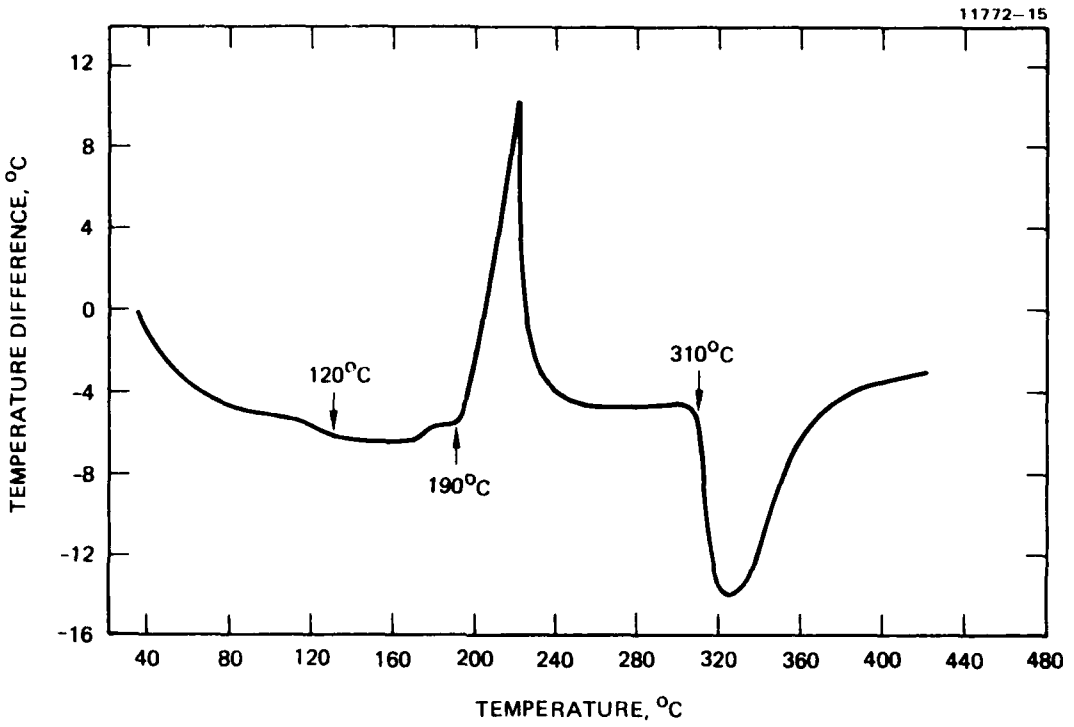

Figure 16. DTA thermogram of RAP $ZnCl_2$ (sealed capsule) showing glass transformation at 120°C, devitrification at 190°C, and fusion at 310°C.

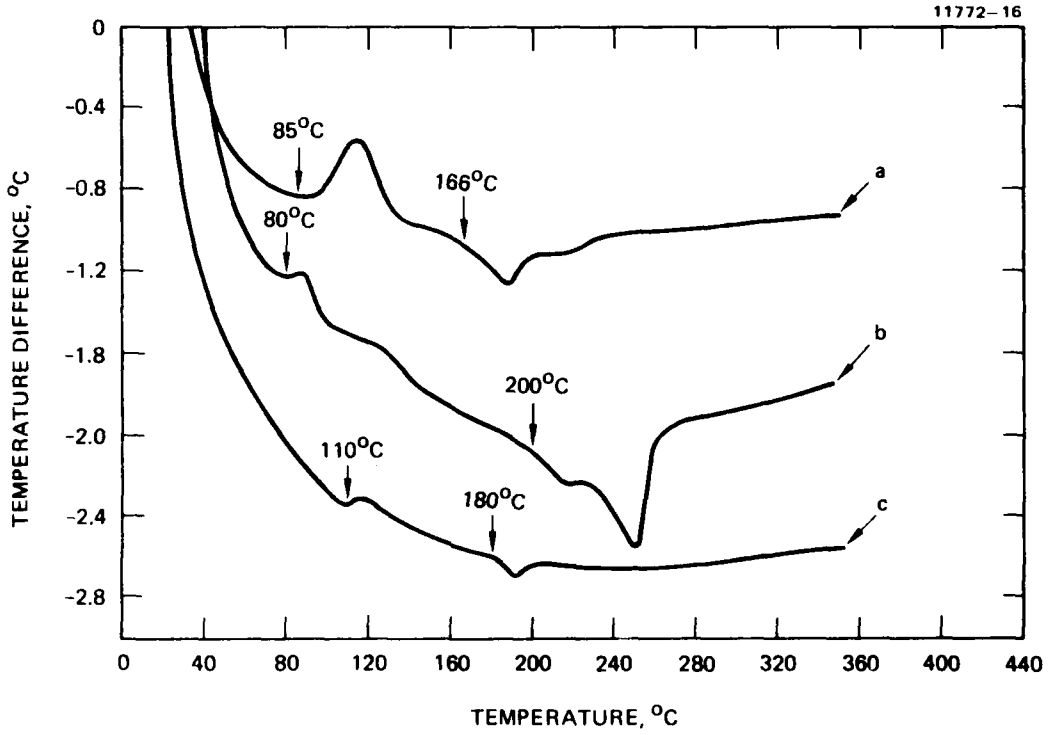

Figure 17. DTA thermograms of non-RAP $ZnCl_2$ in sealed capsule: (a) $ZnCl_2$ with 5 mole % KCl showing T_c at 85°C and T_f at 166°C. (b) $ZnCl_2$ with 2.5 mole % $PbCl_2$ showing T_c at 80°C and T_f at 200°C. (c) 100% $ZnCl_2$ showing T_c at 110°C and T_f at 180°C.

SECTION 4

FUTURE PLANS AND RECOMMENDATIONS

A. EXTRUSION OF THALLIUM HALIDE FIBERS

Our first attempt at extruding clad fiber by coextruding a clad-core billet was unsuccessful. We have decided to abandon this approach in favor of other techniques which appear more promising. One such technique involves sheathing the fiber core after the fiber has been made. In this method, small diameter core is extruded. Then this core is introduced back into a specially designed extrusion die which is used for the application of the sheathing material. The process is analogous to the application of plastic and soft metal (e.g., lead) coatings to wire. In our case, we would first select a hard core and a soft clad because the application of the soft TlBr would hopefully not damage the KRS-5 core. A sheathing die has been designed and is now being fabricated in our machine shop.

Depending on the success of the sheathing technique, we will also begin a serious investigation of the ion-exchange cladding techniques. Particular emphasis will be placed on high temperature ion-exchange because in the past the diffusion process has been too slow when carried out at ambient temperatures.

B. ZINC CHLORIDE GLASS

We plan to improve and further refine the RAP synthesis of $ZnCl_2$ from Zn. In addition, we plan to minimize the tendency to devitrification by doping $ZnCl_2$ with multiple-linkage ions like Ga_2Ge_3, In_2Se_3, and As_2Se_3, as discussed in detail in the text. We will also examine the effect of the nitride (N^{-3}) anion which is close in ion size (1.7 Å) to the chloride (1.8 Å).

We plan to repeat the DTA characterization to determine the enthalpy values associated with the three processes occurring at T_g, T_c, and T_f. If $\Delta H \neq 0$ at T_g, as the work of Scholze on Na_2SiO_3-H_2O glass (Ref. 2) shows, then we must carry out a Thermal Mechanical Analysis (TMA) (dilatometric) study on ΔV at T_g. Scholze's finding differs from the prevalent claim that the T_g-process is a higher order transition.

Knowing ΔH at T_c, we can calculate the $P(H_2O)$ dependence on T of the saturated solution of $ZnCl_2$(vit) from the known dependence of the saturated solution of $ZnCl_2$(crystal). If we know the heat capacity dependence on T for both the vitreous and the crystal forms, then we can calculate the free-energy change for devitrification. Differential scanning calorimeter can yield the desired data, but materials handling is a problem that still has to be figured out.

REFERENCES

1. R.C. Pastor and A.C. Pastor, Mat. Res. Bull 10, 117 (1975).

2. H. Scholze, Glass Ind. 47, 670 (1966).


DATE
FILME
8